THE PENNSYLVANIA STATE UNIVERSITY
SCHREYER HONORS COLLEGE

DEPARTMENT OF ELECTRICAL ENGINEERING

ANALYSIS OF DATA COLLECTION PROCESSES IN SPOTLIGHT-MODE SYNTHETIC APERTURE RADAR AND MAGNETIC RESONANCE IMAGING

DANIEL NADER MIKHAIL
SPRING 2016

A thesis
submitted in partial fulfillment
of the requirements
for a baccalaureate degree
in Electrical Engineering
with honors in Electrical Engineering

Reviewed and approved* by the following:

Kenneth Jenkins
Professor of Electrical Engineering
Thesis Supervisor

Jeffrey Mayer
Associate Professor of Electrical Engineering
Honors Adviser

* Signatures are on file in the Schreyer Honors College.

ABSTRACT

Synthetic Aperture Radar (SAR) is a radar imaging technique that is used to collect data about targets. These targets are typically landscapes, buildings and other planets. Since SAR can operate in any weather condition and during any time of day, it is a useful tool for military and scientific purposes. To collect the data, a radar is placed on one side of an aircraft while the aircraft hovers over the desired target. Spotlight-mode SAR, an operation mode of SAR, is capable of producing high-resolution images of targets as this method focuses only at one area of the target at a time. Magnetic Resonance Imaging (MRI), on the other hand, is a popular medical imaging technique. MRI acquires data to produce images of a body's organs, tissues and skeletal system. The interactions between applied magnetic fields and nuclear spins are used to reconstruct images of a body's internal organs and tissues. This thesis project focuses on the analysis of the data acquisition processes that take place in spotlight-mode SAR and MRI.

TABLE OF CONTENTS

LIST OF FIGURES

LIST OF TABLES

ACKNOWLEDGEMENTS

I would like to dedicate this thesis to my father, mother and brother. My family has provided me with incredible support during the course of my lifetime and I owe all my accomplishments to them.

I would like to thank Dr. Kenneth Jenkins, my thesis supervisor, for his guidance and encouragement during the thesis process. Dr. Jenkins provided me with valuable advice and sources that greatly helped me during my research.

I would also like to thank Dr. Jeffrey Mayer, my honors advisor, for his direction and patience during my time as a Schreyer scholar. Dr. Mayer helped me realize which path, within electrical engineering, I want to pursue.

Chapter 1

Synthetic Aperture Radar Introduction

Synthetic Aperture Radar (SAR) is a type of radar that captures the images of far away targets. These targets are objects such as buildings and landscapes. The unique characteristic of SAR is in its generated high-resolution images. To produce these high-resolution images, SAR utilizes radar antennas. These antennas, usually placed on an aircraft, move over the specified target [2]. Major developments in SAR occurred during World War II, while radar research was taking place. The developments were utilized in "military applications, imaging the earth's surface from space, and commercial applications in airports and weather prediction" [16].

A SAR system can be operated in three different modes: spotlight, stripmap, and scan. This paper will mainly focus on spotlight-mode operation. A common feature between the three modes is that the antenna on the aircraft is oriented such that it has a side-looking view with respect to the flight direction. As shown in Figure 1, spotlight-mode operation gathers information of only one area, "spot", at a time [3]. The angle of orientation of the antenna is gradually altered as the aircraft proceeds in its path. As a result, the same area of a terrain remains as the focus for data collection. The fact that multiple angles are utilized in this process enables the creation of a high-resolution image. Furthermore, spotlight-mode SAR is the preferred method among the three SAR operation modes when a high-resolution image is required [4]. Figure 2 shows a high-resolution image of a terrain that is generated by spotlight-mode SAR. Figure 3 is the surface of Venus captured by a SAR during the U.S. NASA Magellan mission in the 1980's [16].

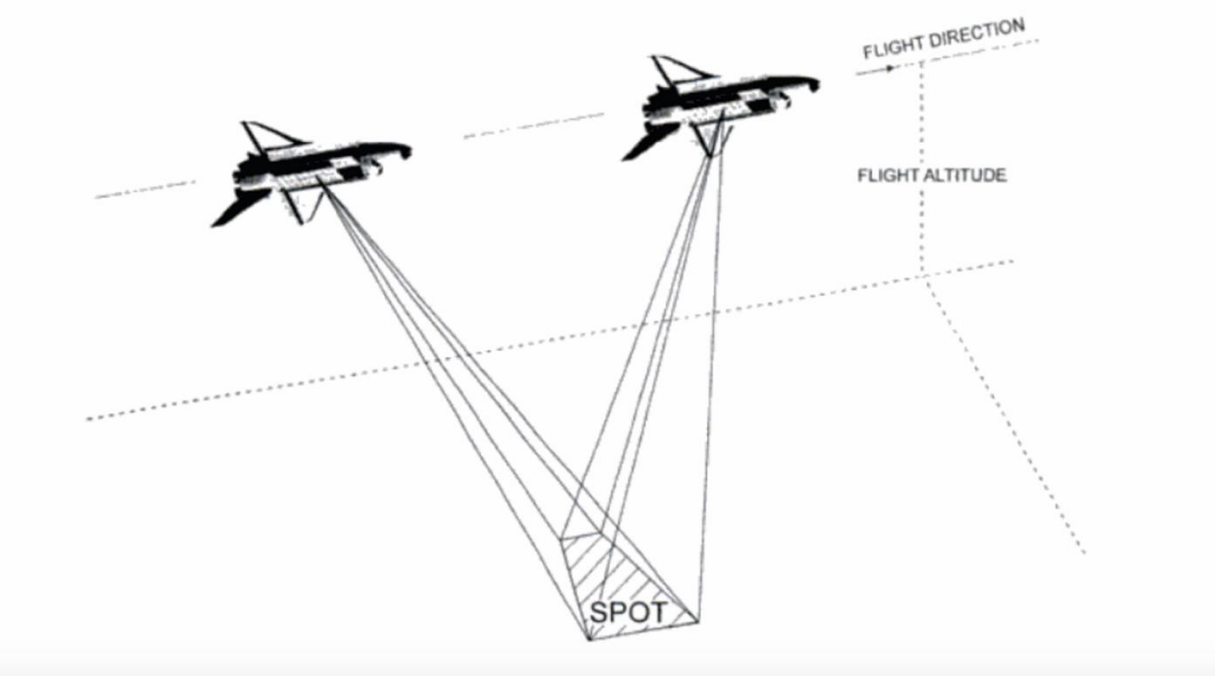

Figure 1: Spotlight-Mode SAR operation [3].

Figure 2: Spotlight-Mode SAR image of an area in Kirtland Air Force Base [5].

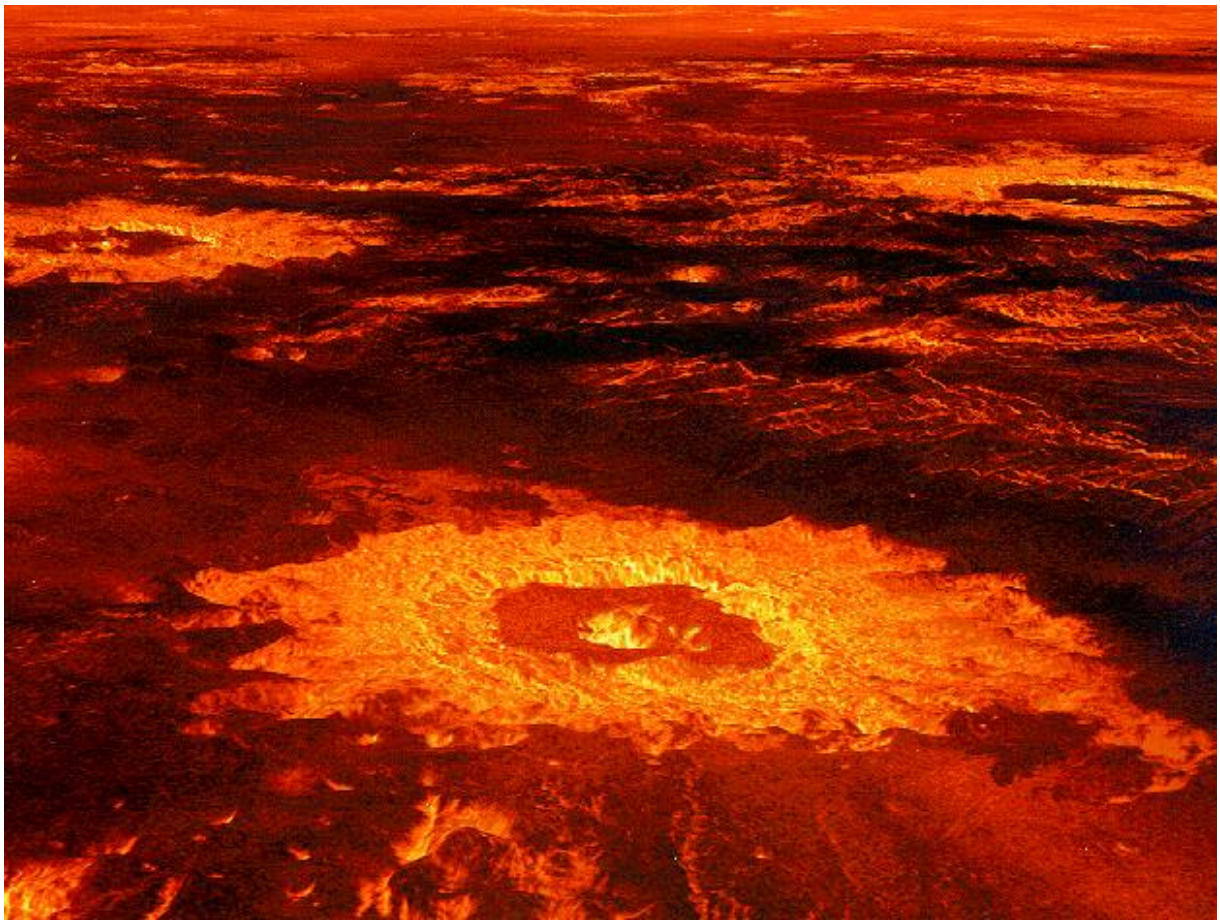

Figure 3: The surface of Venus captured during the U.S. NASA Magellan mission [17].

A significant aspect about SAR is that it can operate in any weather condition during any time of the day. This makes SAR a powerful tool for planet observation [3]. Additionally, SAR is a coherent radar system. A coherent radar is identified by the fact that its transmitted pulse's phase angles have the same reference. As a result of the pulses, data about the target can be stored electronically through transmit/receive cycles. A property of the radar pulses is its pulse repetition frequency (PRF), which is defined as "the number of pulses that are transmitted per second" by a radar system. Equation 1 relates the PRF to a pulse's PRT (pulse-repetition time). The PRT is "the time between the beginning of one pulse and the start of the next pulse [1]

$$PRF = \frac{1}{PRT}. \quad (1)$$

The following chapter analyzes the data collection process in synthetic aperture radar. Chapter 3 introduces the concept of magnetic resonance imaging (MRI) and its main hardware components. Chapter 4 analyzes the data collection process in MRI. Finally, Chapter 5 presents the similarities between the data collection processes in SAR and MRI.

Chapter 2

Analysis of Data Collection Process in SAR

The geometry of spotlight-mode SAR allows for effective data collection. As previously shown, in spotlight-mode SAR, the radar beam illuminates a target. In this chapter, the target will be a ground region. Regardless of antenna size, spotlight-mode SAR collects radar signals from a range of angular views (in the azimuthal range) of the illuminated ground region. The azimuthal range is the horizontal cross-range. During the aircraft's flight, the radar continuously points towards the targeted ground region. Linear FM (frequency modulation) signals (chirp pulses) are transmitted to the ground region at equal angular increments. Echoes, projected views of the targeted region, are then received and processed. A major advantage of utilizing equal angular increments is that the speed of the aircraft does not influence the transmitted signals. SAR would even continue to operate properly in the unlikely case that the aircraft stops during its flight path [4]. This emphasizes SAR's high adaptability to any type of aircraft.

The reflectivity of the illuminated ground region is utilized when the return signal is received. This reflectivity is modeled by a complex function, $g(x, y)$ and is characterized by the expression

$$g(x, y) = |g(x, y))|e^{(j\angle g(x,y)))}, \tag{2}$$

where x and y are the Cartesian coordinates in the azimuthal range of the targeted ground region. The reflectivity function affects both the amplitude and the phase of the return signal. In the instance that a point (x_0, y_0) in the targeted region produces a sinusoidal return signal, the signal

will be amplitude scaled by $|g(x_0, y_0)|$. This amplitude scaling occurs as a result of only a fraction of the initial transmitted signal being received back by the radar. Furthermore, the return signal experiences a phase shift by $\angle|g(x_0, y_0)|$. This phase shift may be due to dielectric differences at the air and ground interface [4]. Eventually, multiple complex reflectivity functions will be returned to the radar. From these returned signals, the magnitude of reflectivity is calculated through SAR's processing system [6].

As the aircraft flies along its path, SAR assumes that a point in the illuminated region is in a linear array. As mentioned earlier, the radar transmits a signal in the form of a linear FM chirp pulse. Pulse compression is used in chirp pulses and produces images that are high in resolution. Pulse compressions do not require large peak power while providing a large bandwidth. Also, its time bandwidth is greater than unity. A linear FM chirp pulse is expressed as

$$s(t) = \begin{cases} e^{j(w_0 t + at^2)}, & |t| \leq \frac{T}{2} \\ 0, & all\ other\ values\ of\ t \end{cases} \tag{3}$$

where w_0 is the carrier frequency, 2a is the FM rate and T is the period of the chirp pulse [6]. The pulse's linear phase is evident in the "w_0t" term of (3). The term in parenthesis of the exponent in (3) is the phase of the pulse.

The chirp pulse exhibits a linear relationship between frequency and time. To explain this concept, let θ, the phase, be a quadratic function,

$$\theta(t) = w_0 t + at^2. \tag{4}$$

Therefore, the derivative of the phase is

$$\frac{d}{dt}\theta(t) = \frac{d}{dt}(w_0 t + at^2) = w_0 + 2at. \quad (5)$$

This derivative term is called a "chirp" and is linear with respect to time. Figure 4 displays the chirp pulse's linear nature. The pulse sweeps through w_0, the carrier frequency. Furthermore, one pulse lasts for one period, T.

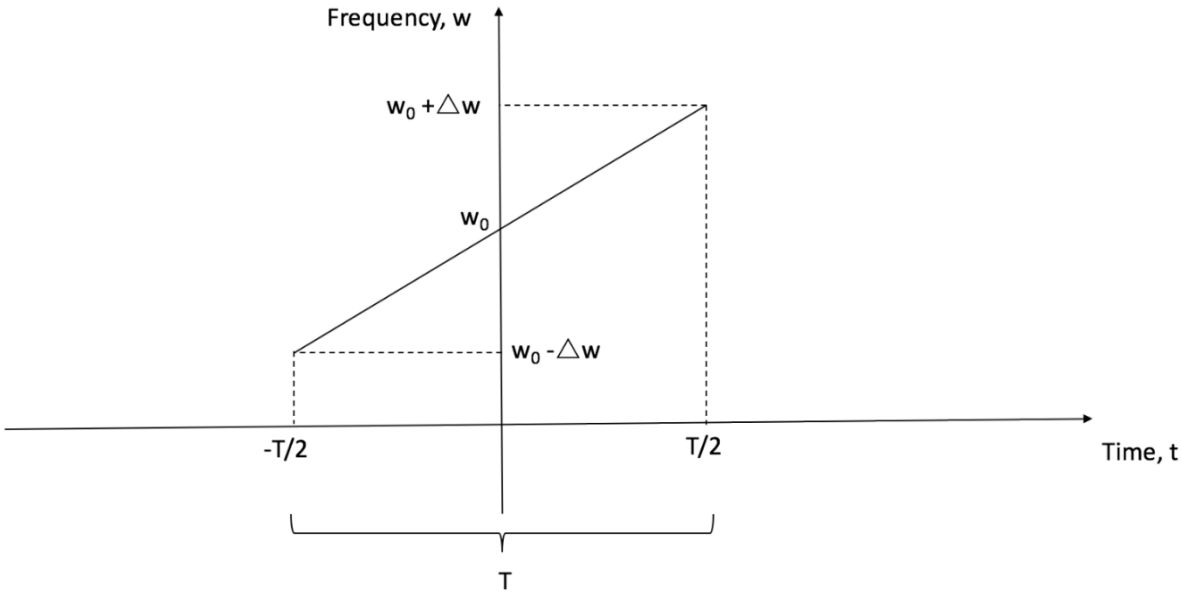

Figure 4: The chirp pulse is a linear FM pulse.

The signal returned to the radar from a small area in the target region is the reflectivity function multiplied by a chirp pulse that is delayed by $2R_0/c$. R_0 is the distance from the point (x_0, y_0) in the center of the small area to the radar and c is the speed of light. The factor of 2 in the delay accounts for the time it takes for the transmitted signal to reach the targeted region plus the time it takes the return signal to arrive at the radar from the targeted region. The return signal is expressed as

$$r_0(t) = Ag(x_0, y_0)s(t - \frac{2R_0}{c}) \tag{6}$$

where A is an attenuation constant. (6) can be expanded to yield

$$r_0(t) = A|g(x_0, y_0)| \cos\left(w_0\left(t - \frac{2R_0}{c}\right) + a\left(t - \frac{2R_0}{c}\right)^2 + \angle g(x_0, y_0) \right) dxdy \tag{7}$$

where dxdy is the differential area in the targeted region where (x_0, y_0) is centered. Finally, (7) can be simplified to give

$$r_0(t) = ARe\left\{g(x_0, y_0)s(t - \tfrac{2R_0}{c})\right\} dxdy. \tag{8}$$

This simplification keeps only the real portion of the return signal. The return signal is then multiplied with a reference chirp and passed through a low-pass filter [6].

For the upcoming analysis, an assumption that is taken into account is that the distance, R, from the radar to the illuminated target is much greater than the radius, L, of the illuminated target. This means that points in the target that are equidistant from the radar will be approximated to be located on a straight line. The geometry of Figure 5 will be used in the mathematical analysis of spotlight-mode SAR.

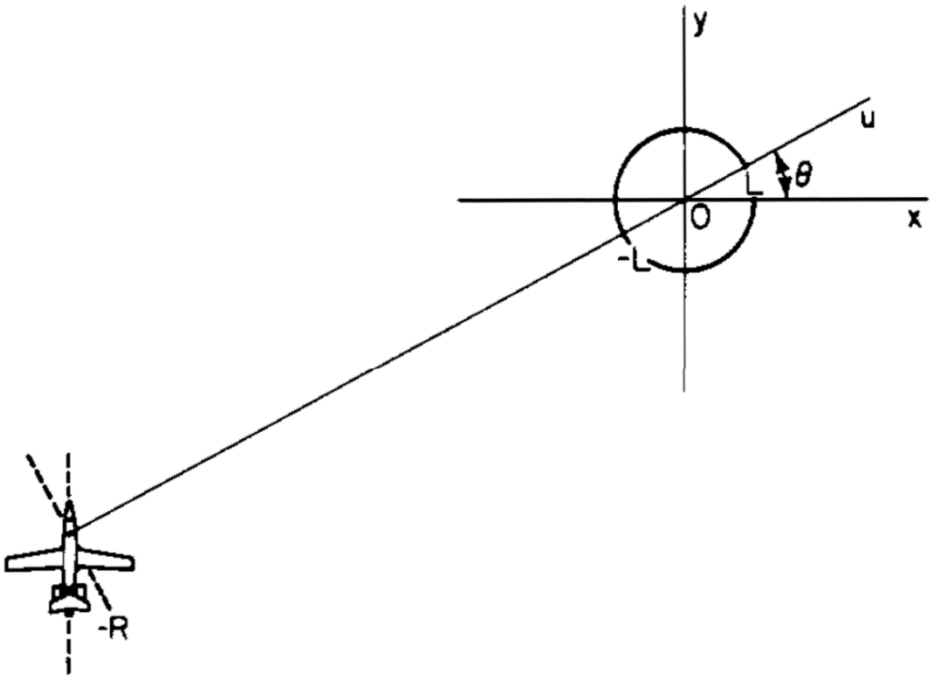

Figure 5: Spotlight-Mode SAR geometry [4].

Using u = u_0 as a line in the Figure 5 configuration, the return signal from this line becomes

$$r_0(t)|_{u=u_0} = ARe\left\{p_\theta(u_0)s(t-\frac{2(R+u_0)}{c})\right\}du \tag{9}$$

where $p_\theta(u_0)$ is the reflectivity function g projected at angle θ and evaluated at line u = u_0. As shown in Figure 5, angle θ is the angle between the x-axis and u-axis. The projected function $p_\theta(u_0)$ is defined as

$$p_\theta(u) = \int_{-\infty}^{\infty} g(ucos\theta - vsin\theta, usin\theta + vcos\theta)dv \tag{10}$$

where the v-axis is a perpendicular axis to the u-axis. Using the assumption mentioned earlier, that R is much greater than L, the attenuation, A, in (9) can be approximated as a constant. As a result, the return signal from the illuminated targeted region can be represented as

$$r_\theta(t) = ARe\left\{\int_{-L}^{L} p_\theta(u_0)s(t-\frac{2(R+u)}{c})\,du\right\}. \quad (11)$$

By substituting the chirp pulse expression (3) into (11), the following return signal is obtained

$$r_\theta(t) = ARe\left\{\int_{-L}^{L} p_\theta(u_0)e^{\left\{j\left[w_0\left(t-\frac{2(R+u)}{c}\right)+a\left(t-\frac{2(R+u)}{c}\right)^2\right]\right\}}\,du\right\} \quad (12)$$

which is valid for

$$-\frac{T}{2}+\frac{2(R+L)}{c} \le t \le \frac{T}{2}+\frac{2(R-L)}{c}. \quad (13)$$

The return signal is then multiplied with the reference chip pulse,

$$s_{ref}(t) = e^{j\left(w_0(t-\tau_0)+a(t-\tau_0)^2\right)}, \quad (14)$$

where

$$\tau_0 = \frac{2R}{c}. \quad (15)$$

After the multiplication, the signal is passed through a low-pass filter, yielding

$$\hat{r}_\theta(t) = \frac{A}{2}Re\left\{\int_{-L}^{L} p_\theta(u)e^{\left\{j\left[\frac{4au^2}{c^2}-\frac{2u}{c}(w_0+2a(t-\tau_0))\right]\right\}}\,du\right\}. \quad (16)$$

As a result, (16) along with its quadrature component forms the complex signal,

$$\bar{C}_\theta(t) = \frac{A}{2}\int_{-L}^{L} p_\theta(u)e^{\left\{-j\frac{2}{c}[w_0+2a(t-\tau_0)]\right\}}\,du. \quad (17)$$

This expression can be further simplified as

$$\bar{C}_\theta(t) = \frac{A}{2} P_\theta \left[\frac{2}{c}\left(w_0 + 2a(t - \tau_0)\right)\right], \quad (18)$$

which has the form of the Fourier transform of the projection function. The meaning behind the processed expression (18) is profound since a slice at angle θ of the 2-D Fourier transform of the reflectivity function g is now represented. Multiple processed signals can now be obtained at different angles to provide information about the reflectivity function in the frequency domain. After the polar samples are obtained, interpolation of the samples to a Cartesian grid takes place. Finally, the inverse 2-D fast Fourier transform is utilized to present the amplitude of the reflectivity function g. The now known reflectivity function provides a display of the illuminated region targeted by spotlight-mode SAR [4, 6].

Chapter 3

Magnetic Resonance Imaging Introduction

Magnetic Resonance Imaging (MRI) is a medical imaging method that is capable of distinguishing between healthy and diseased tissue inside the human body. MRI provides information about the functional and physiological state of the organs. MRI's uniqueness lies in the fact that patients are not exposed to ionizing radiation. This medical imaging technique provides high spatial resolution of a cross-section of an area of the object under test, typically the human body [7, 8].

The behavior of the nuclei in atoms in a magnetic field gives rise to MRI. Nuclei consist of positively charged particles, protons, and particles that have no charge, neutrons. A fundamental property of the nucleus is its intrinsic spin angular momentum (spin). Spin causes nuclei to rotate at a constant velocity about an axis. The direction of the rotation is perpendicular to the axis, as presented in Figure 6. In Figure 6, the curved arrow in the diagram is the direction of the spin and the straight solid arrow is the perpendicular self-rotation axis. As a result of the spin, from the positively charged nucleus, a magnetic field, **B**, is produced. This field, the nucleus' magnetic moment, is parallel to the rotation axis.

When nuclei are placed inside a magnetic field, the nuclei absorb energy when the energy is transmitted at their frequency of precession. Precession is the revolving motion of a proton about an axis, the precessional axis, inside a magnetic field. This precessional axis is parallel to the main magnetic field, as shown in Figure 7. In Figure 7, the magnetic field, $\mathbf{B}_0$, and the precessional axis are parallel to the z-axis, and ω_0 is the frequency of precession.

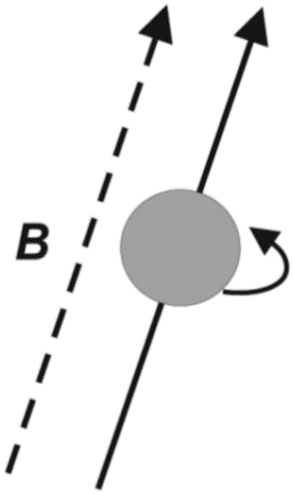

Figure 6: A nucleus' spin produces a magnetic field [9].

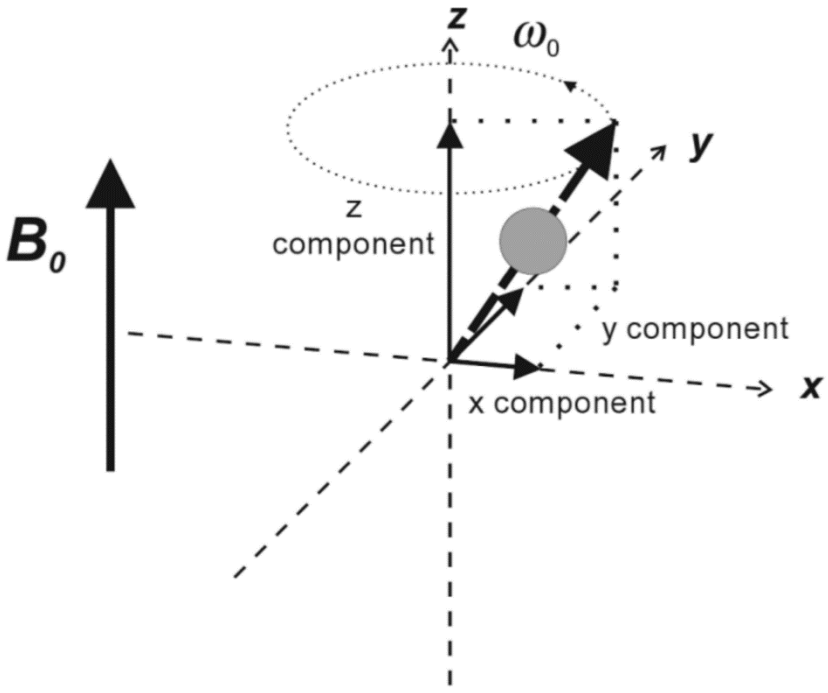

Figure 7: Precession inside a magnetic field [9].

A superconducting magnet, a radio frequency (RF) coil system, and a gradient coil system make up the major hardware components needed to collect information to produce an MRI image [10]. This setup is shown in Figure 8.

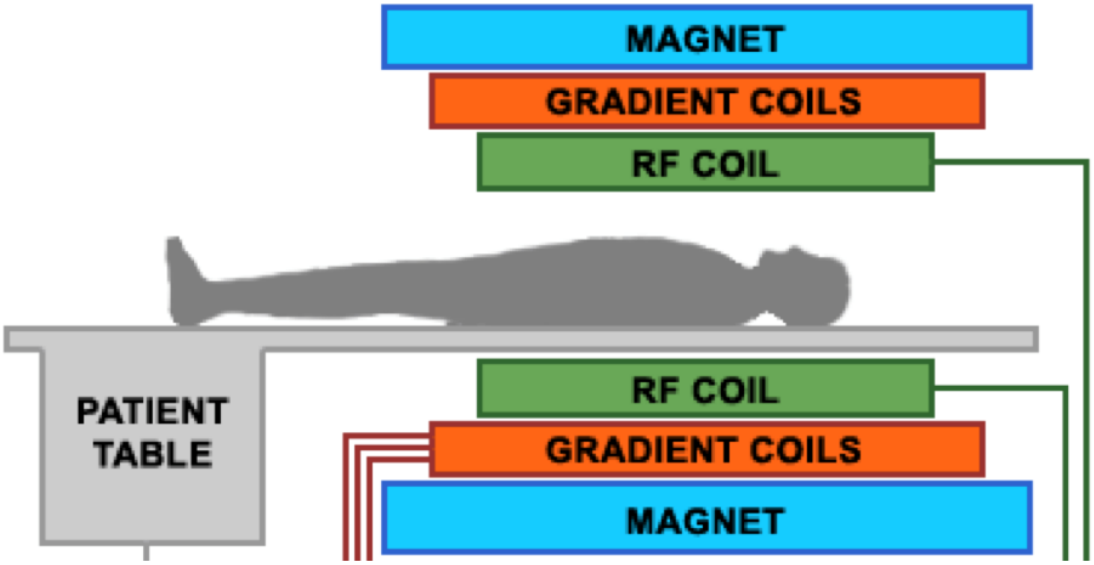

Figure 8: The major hardware components for MRI [11].

As a human is undergoing MRI, a homogeneous magnetic field, $\mathbf{B_0}$, is produced by the superconducting magnet and is sent through the human. After that, an electromagnetic pulse, $\mathbf{B_1(t)}$, is transmitted by RF coils. This pulse is perpendicular to $\mathbf{B_0}$. Eventually, when the transmission of $\mathbf{B_1(t)}$ stops and with the help of gradient coils, the RF receiver coils detect the object's emitted signals. This nuclear magnetic resonance (NMR) data is eventually utilized to reconstruct images of the object under test [10]. The following chapter explains how data is collected to produce an MRI image. Figure 9 is an example of an MRI image of the human body's chest region.

Figure 9: An MRI image of a human's chest region [18].

Chapter 4

Analysis of Data Collection Process in MRI

Hydrogen's one proton nucleus is the main type of nucleus utilized by MRI. This is because it is found in abundance in the human body since the human body is mostly made up of water, H_2O. Generally, the magnetic dipole of any nucleus points in a random direction as long as it is not placed in an external magnetic field. However, when the nuclei are placed in the superconducting magnet's magnetic field, $\mathbf{B}_0$, the magnetic dipoles will orient themselves in such a way that they are aligned in parallel with the direction of $\mathbf{B}_0$ [7, 12].

Superconducting magnets are utilized in MRI as they are capable of producing stable magnetic fields. A superconducting magnet can operate for up to a few months at a constant magnetic field. Furthermore, these magnets can "support a very high current density with a vanishingly small resistance." Therefore, these magnets require low electrical power input [19].

A nucleus' magnetic moment may precess about the uniform magnetic field's axis as a result of the torque exerted by the superconducting magnet's uniform magnetic field. The mathematical relationship between the angular frequency of the precession, the Larmor frequency, and the externally applied static magnetic field is

$$\omega_0 = \gamma B_0, \tag{19}$$

where the constant γ is the atom's gyromagnetic ratio. The gyromagnetic ratio is different for almost all nuclear species [10, 7]. Table 1 presents the gyromagnetic ratios for the four most abundant elements in the human body. For the special cases of Oxygen-16 and Carbon-12, the gyromagnetic ratio is 0, implying that their frequency of precession is also 0.

Table 1: Gyromagnetic Ratios for the human body's most abundant elements [9].

Element	*Gyromagnetic Ratio,* γ **(MHzT^{-1})**
Hydrogen-1	42.5774
Carbon-12	0
Nitrogen-14	3.0777
Oxygen-16	0

The Larmor frequency is a characteristic unique to various materials. On the nuclear level of objects, the nuclei have spins and the Larmor frequency is the unique resonance frequency of the object's spin [13, 8]. For the upcoming derivation, let the magnetic field, $\mathbf{B}_0$, be in the $\hat{z}$ direction. Therefore, the perpendicular external magnetic field, $\mathbf{B}_1\mathbf{(t)}$, applied by RF coils, is

$$\boldsymbol{B}_1(\boldsymbol{t}) = B_1(t)\cos(\omega_{rf} + \varphi)\hat{x}. \tag{20}$$

In order for the nuclei of the atoms of the object under to test to absorb energy from the $\mathbf{B}_1\mathbf{(t)}$ field, the field's frequency of oscillation must match the Larmor frequency. Therefore, the criteria, from (19) and (20), to be satisfied is

$$\omega_{rf} = \omega_0. \tag{21}$$

Under the influence of the $\mathbf{B}_1\mathbf{(t)}$ field, the energy of the atoms increases. However, later, energy is released as a result of the $\mathbf{B}_1\mathbf{(t)}$ field being removed. This energy release occurs when the atoms move from higher energy states to their equilibrium energy states. This energy release leads to the

generation of a nuclear magnetic resonance (NMR) signal. By utilizing Faraday's law, the induced emf of the signal that is detected by the RF receiver coil can be calculated by using the following equation:

$$emf = -\int \frac{\boldsymbol{B}_1}{I_C}\frac{d\boldsymbol{M}}{dt}\, dV. \tag{22}$$

Here, a unit current located at **M**, the net magnetic dipole moment of the object, produces the magnetic field, $\mathbf{B}_1/I_C$. Furthermore, the integral in (22) is evaluated over the sample's volume [8].

The Bloch equation describes the time-dependent nature of **M**. This equation, developed by the physicist Felix Bloch, "provides a model for the interactions between applied magnetic fields and the nuclear spins in the objects under consideration" [13]. The same chemical environment in the same species gives rise to similar spins. The composition of spins, also known as isochromats, in a species is characterized by the spin density function, $\rho(x, y, z)$. The distribution of isochromats in water molecules from hydrogen nuclei is of great importance in the medical field. Using Cartesian coordinates, the 3-vector of the state of the isochromat is represented by

$$\boldsymbol{M}(x, y, z) = (m_1(x, y, z), m_2(x, y, z), m_3(x, y, z)). \tag{23}$$

This is the magnetic moment-per-unit-volume caused by spins within the isochromat. The equilibrium magnetization, which is a bulk magnetic moment, occurs when the spins of a static sample have become polarized. This Polarization typically takes places when the sample is placed in a magnetic field for a long period of time. The equilibrium magnetization is described by the equation

$$\boldsymbol{M}_0(x,y,z) = \chi\rho(x,y,z)\boldsymbol{B}_0(x,y,z), \tag{24}$$

where χ is the nuclear paramagnetic susceptibility of protons. At room temperature, $\chi \approx 3.6 * 10^{-9}$ for water molecules. For an applied magnetic field,

$$\boldsymbol{B} = \boldsymbol{B}_0 + \boldsymbol{B}_1, \tag{25}$$

where the magnitude of the field $\mathbf{B}_0$ is much greater than the magnitude of the field $\mathbf{B}_1$, the Bloch equation is

$$\frac{d\boldsymbol{M}(x,y,z;t)}{dt} = \gamma\boldsymbol{M}(x,y,z;t) \times \boldsymbol{B}(x,y,z;t) - \left(\frac{1}{T_2}\right)\boldsymbol{M}^{\perp}(x,y,z;t) + \left(\frac{1}{T_1}\right)\left(\boldsymbol{M}_0(x,y,z) - \boldsymbol{M}^{\parallel}(x,y,z;t)\right). \tag{26}$$

In (26), $\times$ is the vector cross product, and T_1 and T_2 are time constants. $\boldsymbol{M}^{\perp}(x,y,z;t)$ is the transverse component as this component is perpendicular to $\boldsymbol{B}_0(x,y,z)$ and is a component of $\boldsymbol{M}(x,y,z;t)$. On the other hand, $\boldsymbol{M}^{\parallel}(x,y,z;t)$ is the longitudinal component as this component is parallel to $\boldsymbol{B}_0(x,y,z)$ and is a component of $\boldsymbol{M}(x,y,z;t)$ [8, 13]. The cross product term in (26) describes the precession. The the second term is the transverse decay term and the third and final term is the longitudinal recovery term, both terms are relaxation terms [14, 13].

From an MRI standpoint, the Bloch equation is

$$\frac{d\boldsymbol{M}}{dt} = \gamma\boldsymbol{M} \times (B_0\hat{z} + \boldsymbol{B}_1) - \left(\frac{\boldsymbol{M}_{xy}}{T_2}\right) + \left(\frac{(M_z - M_z^0)}{T_1}\right)\hat{z}, \tag{27}$$

where, under the influence of the $\mathbf{B}_0$ field, M_z^0 is the thermal equilibrium value of **M.** The coefficient in the transverse decay term, $1/T_2$, is the rate of decay of **M**'s transverse components, and the coefficient in the longitudinal recovery term, $1/T_1$, is the rate of return from magnetization

to equilibrium. T_2 values, which are smaller than T_1 values, used in this model are typically between 40ms and 4s. These values are suitable for liquid-like materials as soft tissues in mammals have similar characteristics to liquid-like materials. This Bloch equation model accounts primarily for interactions between isochromats and their environments. The analysis of NMR imaging is based on the behavior of different magnetic **B** fields in the Bloch equation model.

As mentioned earlier, $\mathbf{B}_1\mathbf{(t)}$ is an electromagnetic pulse. This pulse is generated in a pulse sequence, a succession of radio frequency pulses. In MRI, contrast depends on the density of a nucleus' protons. In addition, contrast depends on the parameters of the pulse sequence as these parameters affect the behavior of protons in the nucleus. Examples of the parameters are the echo time, TE, which is the time between the excitation of the NMR signal and the measurement of the NMR signal, and the composition of magnetic gradients [15].

Gradient coils are utilized so that only the desired slice of a body is examined in imaging. This is achieved by encoding spatial information into the NMR signal. In MRI applications, it is assumed that the components of the gradient magnetic fields depend linearly on position, (x, y, z). These fields are in addition to the $\mathbf{B}_0$ and $\mathbf{B}_1\mathbf{(t)}$ fields and their components orthogonal to $\mathbf{B}_0$ are ignored [13, 9]. The Larmor frequency of a nucleus at position i now becomes

$$\omega_i = \gamma(B_0 + \boldsymbol{G} \cdot \hat{r}_i), \tag{28}$$

where $\cdot$ is the dot product, taken between the total gradient vector, **G**, and the position of the nucleus, $\hat{r}_i$ [9]. Taking the gradient vector into account, the Bloch equation in Matrix form is

$$\begin{bmatrix}\dot{M}_x\\ \dot{M}_y\\ \dot{M}_z\end{bmatrix} = \begin{bmatrix}0 & \gamma(B_0 + \boldsymbol{G}\cdot\hat{r}_i) & -\gamma B_{1y}\\ -\gamma(B_0 + \boldsymbol{G}\cdot\hat{r}_i) & 0 & \gamma B_{1x}\\ \gamma B_{1y} & -\gamma B_{1x} & 0\end{bmatrix}\begin{bmatrix}M_x\\ M_y\\ M_z\end{bmatrix}$$

$$+ \begin{bmatrix}-\left(\frac{1}{T_2}\right) & 0 & 0\\ 0 & -\left(\frac{1}{T_2}\right) & 0\\ 0 & 0 & -\left(\frac{1}{T_1}\right)\end{bmatrix}\begin{bmatrix}M_x\\ M_y\\ M_z\end{bmatrix} \tag{29}$$

$$+ \begin{bmatrix}0\\ 0\\ \frac{1}{T_1}\end{bmatrix} M_0.$$

Here, the top term is called the precession term, the second term is the relaxation term and the third term is the recovery term.

In order to produce an image of an object slice, three gradients are applied. These gradients are the slice-selection gradient, the frequency-encoding gradient, and the phase-encoding gradient. The aim of the first gradient, the slice-selection gradient, $\mathbf{G}_{SS}$, is to obtain location and thickness data about the desired object slice. This is achieved by transmitting the $\mathbf{G}_{SS}$ gradient in the same direction as the $\mathbf{B}_0$ field, along the z-axis. The linear relationship between the gradient amplitude and position means that ω_i values can be calculated using (28). As a result, the desired object slice will generate an NMR signal by selecting the corresponding bandwidth of frequencies in the RF pulse, $\mathbf{B}_1(t)$. Figure 10 displays the function of the slice-selection gradient. In the figure, **z** represents the slice location and $\Delta\mathbf{z}$ represents the slice thickness. The purpose of the second gradient, the frequency-encoding gradient, $\mathbf{G}_{FE}$, is to determine the x-position of an NMR signal. After the transmission of $\mathbf{B}_1(t)$ is halted, $\mathbf{G}_{FE}$ is transmitted along the x-axis. Since the amplitude of $\mathbf{G}_{FE}$ varies linearly with position, the nuclei in the desired slice precess at various frequencies.

The third gradient, the phase-encoding gradient, $\mathbf{G}_{PE}$, is transmitted along the y-axis. This gradient uses the phase of an NMR signal to locate the y-positions of nuclei in the object slice. This is achieved by causing the nuclei that have the same precession frequency to have different phase values [9].

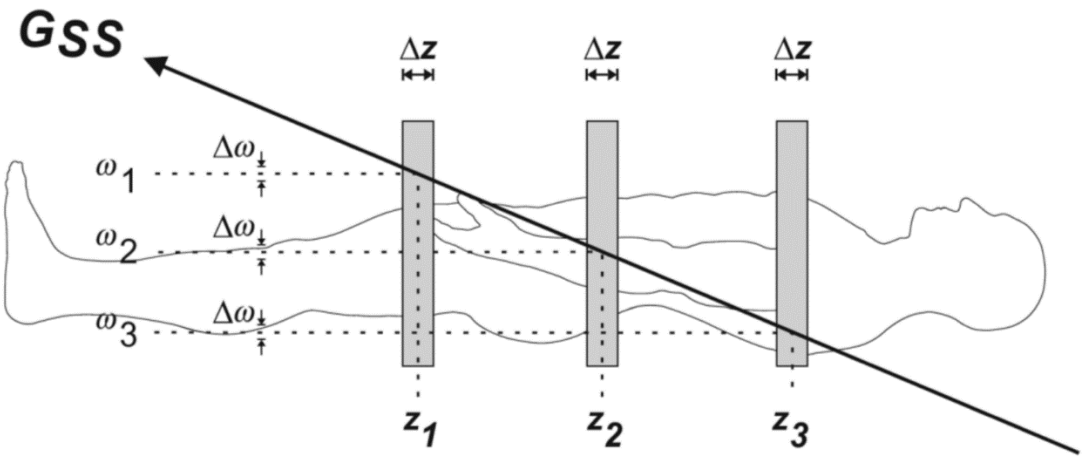

Figure 10: The slice-selection gradient determines the slice thickness [9].

After the object slice data is detected, an image of the object slice is constructed. The data is stored in a k-space matrix, which is sampled data in the Fourier domain. Finally, a 2-D Fourier transform method is typically utilized to produce an image reconstruction. This is created by producing an image function, I(x, y), a representation of the object slice's cross-section from the detected data. The relationship between the image function and the k-space matrix data, $S(k_x, k_y)$, takes on the form of an inverse Fourier transform. This relationship is [10]

$$I(x,y)) = \int_{-\infty}^{\infty}\int_{-\infty}^{\infty} S(k_x,k_y)e^{j2\pi(k_x x + k_y y)}dxdy. \quad (30)$$

Chapter 5

Conclusions

Even though spotlight-mode SAR and MRI are utilized in different applications, SAR being used in reproducing images of targets such as landscapes and planets while MRI is used in medical applications to produce images of the human body's internal organs and tissues, there are similarities that can be drawn between the two methods' data collection process. One similarity between the two methods is that high resolution images are ultimately produced. In spotlight-mode SAR, this is achieved by focusing radar signals at only one area of the targeted region at a time. On the other hand, by analyzing atomic behavior, MRI provides high spatial resolution, contrast between soft tissues, and information about the functional state of organs.

Adaptability is another similarity between SAR and MRI. SAR can operate in any weather condition during any time of day, while MRI images can be created at any orientation of the magnetic fields. This is because the nuclei's magnetic dipoles will orient themselves in such a way that they are aligned in parallel with the direction of $\mathbf{B}_0$. A difference between SAR and MRI is in the way signals are generated. In SAR, the signals, chirp pulses, are generated externally. The signals, after being transmitted by the radar, are returned back from the target and then used to create an image. However, in MRI, the signals are generated internally, from within the object under test. The nuclear magnetic resonance (NMR) signal is generated as result of energy released from the movement of atoms higher energy states to their equilibrium energy states.

In SAR, the reflectivity function of the targeted region serves a similar role as the spin density function in MRI. The reflectivity function affects the amplitude and phase of the signal returned from the targeted region. Ultimately, this leads to the reconstruction of an image as the image's contrast depends on the reflectivity density of the targeted region. Similarly, in MRI, the

composition of spins, characterized by the spin density function affects the reconstructed image. This is because image contrast depends on the density and behavior of the nuclei's protons.

A final similarity between the two methods is the utilization of the 2-D Fourier transform. In SAR, slices at different angles of the 2-D Fourier transform of the reflectivity function g are represented. Therefore, by using the inverse 2-D fast Fourier transform to present the amplitude of the reflectivity function g, a display of the illuminated targeted region can be produced. Similarly, in MRI, after object slice data has been detected the sampled data is in the Fourier domain. Then, by using this data and a 2-D Fourier transform method an image function and, ultimately, an image are produced.

BIBLIOGRAPHY

[1] Stimson, George W. *Introduction to Airborne Radar.* 2nd ed. Mendham: SciTech, 1998. Print.

[2] "Synthetic Aperture Radar." *Radar Basics.* Christian Wolff. Web. 26 Jan. 2016. <http://www.radartutorial.eu/20.airborne/ab07.en.html>.

[3] Franceschetti, Giorgio, and Riccardo Lanari. *Synthetic Aperture Radar Processing.* Boca Raton: CRC, 1999. Print.

[4] Munson, David C., Jr., James D. O'Brien, and W. Kenneth Jenkins. "A Tomographic Formulation of Spotlight-Mode Synthetic Aperture Radar." *Proc. IEEE* 71.8 (1983): 917-25. Print.

[5] "Synthetic Aperture Radar (SAR) Imagery." *Sandia National Laboratories.* Sandia Corporation. Web. 02 Feb. 2016. <http://www.sandia.gov/RADAR/imagery/index.html>.

[6] Desai, Mita D. *A NEW METHOD OF SYNTHETIC APERTURE RADAR IMAGE RECONSTRUCTION USING MODIFIED CONVOLUTION BACK-PROJECTION ALGORITHM.* Thesis. University of Illinois at Urbana-Champaign, 1985. Print.

[7] Pykett, Ian L. "NMR Imaging in Medicine." *Scientific American* 246.5 (1982): 78-88. Web.

[8] Kuperman, Vadim. *Magnetic Resonance Imaging: Physical Principles and Applications.* San Diego: Academic, 2000. Print.

[9] Brown, Mark A., and Richard C. Semelka. *MRI Basic Principles and Applications.* Hoboken: Wiley-Blackwell, 2010. Print.

[10] Liang, Zhi-Pei, and Paul C. Lauterbur. *Principles of Magnetic Resonance Imaging: A Signal Processing Perspective.* Bellingham: SPIE Optical Engineering, 2000. Print.

[11] "Incremental Encoders for Magnetic Resonance Imaging & Precise Position Measurement/Display Control." *DYNAPAR.* Dynapar. Web. 27 Mar. 2016. <https://www.dynapar.com/Products/Industry_Solutions/Medical_/_Life_Sciences/>.

[12] Smith, Hans- Jørgen, and Frank N. Ranallo. *A Non-Mathematical Approach to Basic MRI.* Madison: Medical Physics Pub., 1989. Print.

[13] Epstein, Charles L., and Felix W. Wehrli. *Magnetic Resonance Imaging*. University of Pennsylvania, 3 June 2005. Web. 10 Feb. 2016. <https://www.math.upenn.edu/~cle/papers/nmri_sngl.pdf>.

[14] Lusting, Miki. "Principles of MRI." University of California, Berkeley. Web. 10 Feb. 2016. <https://inst.eecs.berkeley.edu/~ee225e/sp12/notes/Lecture10_021612_4.pdf>.

[15] Weishaupt, Dominik, Victor D. Köchli, and Borut Marincek. *How Does MRI Work?: An Introduction to the Physics and Function of Magnetic Resonance Imaging*. Berlin: Springer, 2003. Print.

[16] Jenkins, W. K. *Interdisciplinary History of CAS Image Processing.* 2016 International Symposium on Circuits and Systems, Montreal, Canada, to appear.

[17] *3-D Perspective of Three Craters on Venus*. 29 Oct. 1991. Web. 06 Apr. 2016. <http://www2.jpl.nasa.gov/magellan/image7.html>.

[18] "Magnetic Resonance Imaging - Clinical Images." *Siemens*. Siemens Healthcare. Web. 08 Apr. 2016. <http://www.healthcare.siemens.com/magnetic-resonance-imaging/magnetom-world/toolkit/clinical-images?SYSTEM=hwem_global:576>.

[19] "Characteristics of Superconducting Magnets." *American Magnetics*. American Magnetics Inc., 2012. Web. 08 Apr. 2016. <http://www.americanmagnetics.com/charactr.php>.

ACADEMIC VITA

Daniel Mikhail

danielmikhail95@gmail.com

EDUCATION

Bachelor of Science, Electrical Engineering May 2016
The Pennsylvania State University, University Park, PA
Schreyer Honors College
Dean's List (7/7 semesters)

Relevant Courses

Power Electronics	Introduction to Linear Control Systems
Engineering Electromagnetics	Discrete-Time Linear Systems
Introduction to Nanoelectronics	Continuous-Time Linear Systems
Electronic Circuit Design I	Communication Systems I
Circuits and Devices	Programming for Engineers with C++
Design Process	Digital Design: Theory and Practice
Design Tools	Engineering Design

EXPERIENCE

Lutron Electronics Co., Inc. Coopersburg, PA
Electrical Engineering Intern Summer 2015

- Created and documented a procedure that improves the aesthetic performance of 100% to 1% dimmable LED drivers
- Led aesthetic review meetings to evaluate LED driver performance
- Collaborated with standards managers to create a new procedure proposal for the California Energy Commission
- Calculated inductor specifications for a low power LED driver
- Studied the circuitry used in 100% to 1% dimmable LED drivers
- Bench tested LED drivers during the product development phase
- Composed a size analysis of electrical components in 100% to 1% dimmable LED drivers
- Documented an analysis of competitor products

Mercedes-Benz, Egyptian German Automotive Co. Cairo, Egypt
Electrical Maintenance Intern Summer 2013

- Inspected electrical components of CNC machines used in the production of brake discs
- Created weekly preventative maintenance work orders using spreadsheets in Microsoft Excel
- Analyzed PLC ladder diagrams used in the manufacturing of brake discs
- Maintained currency of Siemens S7 PLC program
- Learned the importance of maintenance management in a 24-hour operating factory

ACTIVITIES

- Tau Beta Pi Honor Society, Member Fall 2014 - Present
  - Top 1/8 of third year engineering majors
- Eta Kappa Nu Honor Society, Member Fall 2014 - Present
  - Top 1/4 of third year electrical and computer engineering majors
- THON Hospitality Committee Member Fall 2014 - Spring 2015
- Orphanage Service in Cairo, Egypt Summer 2013
- The National Society of Collegiate Scholars, Member Spring 2013 - Present
- Homeless Service in Redding, CA Fall 2011 - Spring 2012

SKILLS

- C/C++, MATLAB and R programming
- NI Certified LabVIEW Associate Developer (CLAD)
- Multisim, SolidWorks, Microsoft Office
- Arabic (native speaker), English (fluent), Spanish (good working knowledge)